

Quenching star formation in cluster galaxies

Dan S. Taranu^{1,2}, Michael J. Hudson^{2,3}, Michael L. Balogh², Russell J. Smith⁴,
Chris Power⁵, Brad Krane²

¹*Department of Astronomy & Astrophysics, University of Toronto, 50 St. George Street, Toronto, ON, Canada, M5S 3H4.*

²*Department of Physics and Astronomy, University of Waterloo, 200 University Avenue West, Waterloo, ON, Canada, N2L 3G1.*

³*Perimeter Institute for Theoretical Physics, 31 Caroline St. N., Waterloo, ON, N2L 2Y5, Canada.*

⁴*Department of Physics, University of Durham, Science Laboratories, South Road, Durham DH1 3LE.*

⁵*International Centre for Radio Astronomy Research, The University of Western Australia, 35 Stirling Highway, Crawley, WA 6009, Australia.*

21 March 2019

ABSTRACT

In order to understand the processes that quench star formation within rich clusters, we construct a library of subhalo orbits drawn from Λ CDM cosmological N-body simulations of four rich clusters. The orbits are combined with models of star formation followed by quenching in the cluster environment to predict colours and spectroscopic line indices of satellite galaxies. Simple models with only halo mass-dependent quenching and without environmental (i.e. cluster-dependent) quenching fail to reproduce the observed cluster-centric colour and absorption linestrength gradients. Models in which star formation is instantly quenched at the virial radius also fail to match the observations. Better matches to the data are achieved by more complicated bulge-disc models in which the bulge stellar populations depend only on the galaxy subhalo mass while the disc quenching depends on the cluster environment. In the most successful models quenching begins at pericentre, operating on an exponential timescale of 2 – 3 Gyr, with the shorter timescale being a better match to disc colours as a function of cluster-centric radius and the longer being a better fit to the radial dependence of stellar absorption line indices. The models thus imply that the environments of rich clusters must impact star formation rates of infalling galaxies on relatively long timescales - several times longer than a typical halo spends within the virial radius of a cluster. This scenario favours gentler quenching mechanisms such as slow “strangulation” over more rapid ram-pressure stripping.

Key words: galaxies: clusters: general – galaxies: formation – galaxies: evolution – galaxies: haloes – galaxies: star formation.

1 INTRODUCTION

Understanding the physical mechanisms that halt star formation has been a long-standing challenge in galaxy formation and evolution. It is clear from the colour-magnitude relation (Sandage & Visvanathan 1978; Bower et al. 1992) that mass or, more accurately, velocity dispersion (Smith et al. 2009a; Graves et al. 2009) is a driving parameter of the stellar populations in red galaxies. At the same time, the morphology–density (Hubble & Humason 1931; Dressler 1980; Postman & Geller 1984), the colour–density (Balogh et al. 2004; Hogg et al. 2004) and the age–density (Smith et al. 2006) relations are strong evidence of the role of environment. The latter suggest that environment “quenches” star formation, moving galaxies from the blue cloud to the red sequence. Here quenching is a term

meant to be evocative of or analogous to cooling a hot object. Quenching can be abrupt, as in a small campfire doused by buckets of water, or operate on longer timescales, as in cooling molten hot iron in a pool of water. It has become common to model both an “internal” quenching mechanism (assumed to be tied to galaxy mass) as well as environmental quenching when a galaxy falls into a higher mass halo and becomes a satellite (Kauffmann et al. 1993; Cole et al. 2000; van den Bosch et al. 2008; Weinmann et al. 2009; Peng et al. 2010, 2011; Wetzel et al. 2012b).

Many mechanisms that might quench star formation in cluster environments have been proposed: ram-pressure stripping of the cold gas (Gunn & Gott 1972; Abadi et al. 1999), the removal of the hot gas halo (Larson et al. 1980), sometimes known as “strangulation” (Balogh & Morris 2000) either via ram-pressure (McCarthy et al. 2008) or

via tidal stripping by the cluster potential (Merritt 1984; Mamon 1987), or by “harassment” – encounters with other galaxies (Gallagher & Ostriker 1972; Moore et al. 1998). The ram-pressure stripping and strangulation mechanisms remove the gas that is the fuel for star formation, and so the stellar disc will dim and redden as its stars age. Several of the processes affecting late-type galaxies have been reviewed by Boselli & Gavazzi (2006).

It has long been known that spiral galaxies in the cores of rich clusters are deficient in HI (Davies & Lewis 1973; Haynes et al. 1984; Giovanelli & Haynes 1985; Solanes et al. 2001) and stripping of star-forming gas has been observed in nearby rich clusters (Koopmann & Kenney 2004; Sun et al. 2007; Yagi et al. 2007; Yoshida et al. 2008; Smith et al. 2010; Sivanandam et al. 2010), usually appearing to strip gas on short (several hundred Myr) timescales, but it is unclear if this is dominant quenching mechanism. Other, less abrupt or “gentler” mechanisms such as strangulation or tidal stripping are more difficult to observe. To determine which mechanisms are dominant, one might instead tackle the following more empirical questions: At what location in the cluster or group does quenching first occur? What is the timescale of quenching - is quenching abrupt, ending all star formation within tens of millions of years, or does star formation slowly decline over billions of years? What range of satellite galaxy masses are effectively quenched by the environment? Are all morphological components quenched equally, or, for example, are bulges insensitive to environment while discs are quenched?

A common approach to understanding these processes is semi-analytic modelling (SAMs for short; see Baugh (2006) for a review). SAMs attempt to model important physical process via simple analytical prescriptions, combining these with results from numerical experiments like N-body simulations (hence the semi). A disadvantage of the SAM approach when applied to all galaxy populations is that it is difficult to isolate and study specific environments and physical processes, particularly with a large number of potentially correlated free parameters and physical processes. It is also challenging to determine if the parameterizations of physical processes are themselves appropriate, since a wide range of values for the free parameters can allow for spurious, unphysical good fits to some observables. An alternative approach is to focus on a particular environment with a more specific set of observables allowing for a limited number of mechanisms and prescriptions.

In this paper, we will examine the link between star formation rates and the cluster environment. Previous models of galaxy evolution in a clusters (Balogh et al. 2000; Diaferio et al. 2001, and references therein) employed models linking star formation rates with gas consumption, and in some cases, replenishment (Weinmann et al. 2010). More recent studies (Berrier et al. 2009; McGee et al. 2009; Smith et al. 2012) have focused on pre-processing in galaxy groups. While these approaches have been successful in reproducing star formation rates (SFR) and colour gradients, they have not yet isolated the mechanism responsible for halting star formation despite including a wide variety of models for physical processes. We instead seek to produce models that employ an easily-tested causal connection between environment (traced by infall into a rich cluster) and the evolution of an individual galaxy (see Mahajan et al.

(2011) for a recent example of star formation models of cluster galaxies).

Rather than making an *ab initio* prediction of the total stellar mass content in each galaxy, as in most SAMs, we assign stellar masses by matching dark matter halo velocity dispersions to stellar velocity dispersions. The advantage of this approach is that the free parameters in our models can be given arbitrary values while still ensuring that each halo contains a galaxy of an appropriate stellar mass. We can thus assign arbitrary values to free parameters and indeed use any appropriate parameterization of star formation. However, each model is not guaranteed to predict appropriate star formation histories for each galaxy, so our models are permitted to fail in reproducing some observations, unlike in most SAMs where the free parameters are tuned to reproduce many more observations. One drawback to this approach is that it is difficult to model arbitrarily large numbers of physical processes without an automated parameter search. This issue can be avoided by limiting the models to a very specific environment like rich galaxy clusters. If the stellar populations of cluster galaxies are deeply linked to their environment, one would expect star formation histories quenched by the cluster environment to successfully reproduce cluster-centric radial colour and line index gradients. Conversely, if the cluster environment plays a limited role, models linking evolution to internal properties of a galaxy should more closely match observed data.

In our models, galaxies are assumed to be forming stars until quenched by one of two mechanisms. In one scenario, “internal” quenching of star formation occurs at a time which is assumed to be a function of galaxy velocity dispersion, such that galaxies with high velocity dispersions are internally truncated earlier (see Section 4.1.1 for details of our particular implementation). In the alternative scenario, environmental quenching of star formation occurs in the galaxy when its halo crosses some multiple of the virial radius of the cluster, with an option to delay quenching until the galaxy reaches pericentre or for some fixed time after infall. Though these implementations depict an overly simplified view of galaxy evolution, testing models based upon these mechanisms should provide clues as to the relative importance of environments in star formation. By varying the quenching radius of the cluster we also aim to test the range at which environmental quenching would need to be effective to reproduce observations.

Most models to date have compared predictions with observations of galaxy luminosities and colours. However, the well-known degeneracies between age, metallicity and α -element enhancement can only be broken by using spectroscopic absorption lines sensitive to these three parameters. Our aim is to break these degeneracies by comparing our data to observations of stellar absorption linestrengths in cluster galaxies. In this paper, we focus on colour and absorption linestrength data from the NOAO Fundamental Plane Survey (Smith et al. 2004, hereafter NFPS) of galaxies in rich clusters.

This paper is structured as follows. Section 2 details the simulations used and presents information on the simulated clusters. Section 3 describes the NFPS data in more detail. Section 4 describes the star formation models employed and the results of applying these models to galaxies. We discuss

the implications of our results in Section 5 and summarize and conclude in Section 6.

2 N-BODY SIMULATIONS AND HALO ORBITS

2.1 Methods

The simulation data consists of four rich clusters obtained using the publicly available parallel Tree-PM code GADGET-2 (Springel 2005). Cluster candidates were identified from a low-resolution initial simulation using 256³ particles in a cube of side length 512 h^{-1} Mpc. Λ CDM cosmological parameters $\Omega_\Lambda = 0.72$, $\Omega_m = 0.28$, $h = 0.72$ and $\sigma_8 = 0.8$ were adopted, consistent with WMAP 7-year results (Komatsu et al. 2011). Five candidate clusters were chosen for a higher-resolution re-simulation of 150 approximately equally-spaced time steps from $z = 3$ to $z = 0$. Of these five clusters, four were chosen for the final sample, with one candidate excluded due to a complex merger event between two massive clusters. The remaining four were re-simulated with the ‘zoom’ technique (Katz & White 1993; Navarro & White 1994; Power et al. 2003). In brief, only particles passing near the central overdensity in each simulation are fully sampled. Particles which remain sufficiently far (in practice, more than about 20 Mpc/h) are subsampled and given higher masses to provide an accurate tidal field, with four levels of refinement up to the full 512 h^{-1} Mpc side box. Each re-simulation has 12.5 million dark particles, 8.8 million of which are full resolution with a mass of $6.16 \times 10^8 M_\odot/h$. The particle mass and minimum gravitational softening length of $1h^{-1}$ kpc are sufficient to resolve a Milky Way or M31 mass halo with at least 1,000 particles and achieve a resolution limit of 30 particles per halo for halos close to the total mass of a dwarf galaxy like the Large Magellanic Cloud.

The masses and other physical properties of each cluster at $z = 0$ are given in Table 1. Subhalo catalogues at each time step were generated using the AMIGA Halo Finder (Knollmann & Knebe 2009, hereafter AHF). AHF calculates isodensity contours on an adaptive mesh grid and identifies subhalos as collections of mutually bound particles within unambiguous density contours (i.e. overdensities). The resulting subhalo statistics are for the simulated clusters are given in Table 1. AHF determines halo sizes from upturns in radial density contours, using an iterative process to remove unbound particles. We create halo merger trees by linking between consecutive snapshots’ subhalo catalogues.

A typical problem with N-body simulations of dissipationless dark matter is the overmerging of low-mass dark matter subhalos as they are tidally disrupted by the cluster. This effect has been shown to be at the least strongly resolution-dependent (Moore et al. 1996), and mostly likely an artifact of poor resolution (Klypin et al. 1999). A common solution to this ‘overmerging’ problem, adopted here, is to use the most bound particle to track the orbits of these ‘orphan’ haloes (Kauffmann et al. 1999; Springel et al. 2001). In our implementation, any halo which is detected in at least one snapshot is tracked through its most bound particles in all subsequent snapshots, even if it is not detected again by AHF. Thus once a halo is detected at high redshift,

M_{vir} $10^{14} M_\odot/h$	R_{200} Mpc/h	σ_{1D} km s $^{-1}$	N_P ^a 10^6	N_H ^b	N_I ^c	N_B ^d
17.90	1.98	1176	2.9	33567	9328	1000
13.89	1.82	1103	2.3	32605	6468	1437
9.11	1.58	1073	2.7	30940	7511	1071
9.82	1.62	945	1.6	32980	4800	989

^a Millions of particles within the virial radius of the cluster

^b Number of halos ever tracked, including recovered ‘orphan’ halos.

^c Number of halos which have ever crossed the virial radius of the cluster.

^d Number of halos which crossed the virial radius but are now outside of it.

Table 1. Properties of the four simulated rich clusters and their subhalo populations at $z = 0$.

it is guaranteed to still be present in the final $z=0$ snapshot. Although AHF is capable of detecting most of the massive subhalos in the simulation, the most bound particle tracking technique recovers on average four times as many halos as in the original halo AHF catalogue.

Although this method recovers many genuinely independent subhalos, a side effect is that subhalos are effectively prevented from merging. This is not an unreasonable assumption for most field galaxies falling directly in to a rich cluster. The large velocity dispersion in clusters will suppress mergers and the dynamical friction timescale is long enough that satellites can survive for billions of years (Tormen et al. 1998), unlike in lower mass clusters (Tormen 1997). It is probably not a safe assumption for halos in smaller groups and likely results in an overestimate in the number of subhalos near the cluster center, which could well have actually merged. Besides tracking overmerged halos, we use the most bound particles to fill in ‘gaps’ in each halo’s orbital history, e.g. for halos detected in the 8th and 10th snapshot but not the 9th. Such gaps can occur when a halo crosses a particularly dense region of the cluster, temporarily evading detection before re-emerging in a less dense neighbourhood after pericentre.

In this paper, we will typically define ‘infall’ to occur when the subhalo crosses the radius r_{200} , defined to be the radius at which the density exceeds the critical density, or in some models at a smaller fraction of r_{200} . The lookback time at the first r_{200} -crossing is noted as $t_{r_{200}}$. The orbits allow us to also define the lookback time to first pericentre passage, t_{per} . For the rich clusters studied here, we find that typically t_{per} occurs approximately 0.5 Gyr after $t_{r_{200}}$. t_{per} grows roughly linearly with time as the cluster’s dynamical time grows. Recently ‘infallen’ halos take closer to 0.8 Gyr to reach pericentre on average, as the virial radius of typical clusters grows faster than the velocity dispersion. In principle, pericentre can occur anywhere within r_{200} ; in practice, few halos pass closer than $0.1r_{200}$. The median pericentre is $0.4r_{200}$ with no dependence on t_{infall} except at very low redshift (Fig. 1), where it appears to dip to $0.3r_{200}$.

In addition to tracking subhalo positions and velocities after infall, bound particles are used to compute velocity dispersions for each subhalo. Subhalos are assigned a *maximum* velocity dispersion σ_{max} corresponding to the velocity dis-

persion at the time when the subhalo had the largest mass (and in turn had the largest amount of bound particles) prior to infall within r_{200} . This is based on the assumption that a subhalo will not grow significantly after infall, which is expected to be true. In the real universe, we might expect the galaxy’s baryonic component, which has dissipated and become more tightly-bound, to be much less sensitive to tidal disruption than a dissipationless dark matter halo. Thus the maximum pre-infall halo velocity dispersion serves as a proxy for the (post-infall) stellar velocity dispersion (Conroy et al. 2006), which in turn is the primary driver of the stellar populations (see Section 4 below).

The simulations allow us to mimic observational samples by viewing the subhalos positions and velocities in projection. In all plots of projected quantities, we use the three axial projections of each cluster and appropriate line-of-sight velocities and velocity dispersions to average over projection effects and improve galaxy statistics. We denote the projected radius on the sky as R , to distinguish it from the 3D radius r . We also apply cuts in velocity-space, including all subhalos with velocity cz within $\pm 3\sigma_{cl}$ of the cluster’s mean \bar{cz} . Thus in the plots shown in projection, about 17 percent of the plotted subhalos have $R < r_{200}$ although in 3D they are outside the virial radius ($r > r_{200}$). This fraction can vary from 12-20 percent with velocity dispersion or infall-time related cuts, which we will apply when populating halos with galaxies in Section 4. For a more detailed discussion of contamination due to projection, see Mamon et al. (2010).

2.2 Results

We now examine cluster-centric trends of the two key subhalo properties to be passed to our galaxy evolution code in Section 4: subhalo velocity dispersion σ_{max} and infall/pericentre time. In our models, these two quantities will determine the star formation history of the galaxy stellar populations. These quantities are entirely determined by the dynamics of the dark matter, as long as the assumption of a strict correlation between subhalo velocity dispersion and stellar velocity dispersion holds. Although this is challenging to prove observationally, it is unlikely to be far from true given that most early-type galaxies are dynamically relaxed and have been found to have nearly isothermal total density profiles (Auger et al. 2010).

Fig. 1 shows the distribution of subhalo infall times past r_{200} as a function of both projected and real distance to the centre of each cluster. Most recent infallen halos (< 2 Gyr) are clustered around the same position for any given infall time, likely because most halos have mostly radial orbits and thus have similar infall histories. The majority of intermediate (2-4 Gyr) infallen halos are at large radii, even outside the virial radius of the cluster and thus form a “backsplash” population of galaxies that fell in and back out of the cluster. Few backsplash galaxies remain so longer than 6 Gyr; such old infallen halos are concentrated near the centre of the cluster. This virialized population of subhalos outnumber the very recent infalls within $0.25r_{200}$. At $0.5r_{200}$, the median infall time of a subhalo is barely 2 Gyr.

When considering only infallen halos, the backsplash population dominates at large radii ($> 0.5r_{200}$) and the median infall time increases once again. However, when includ-

ing all halos (not just those that have fallen in), the median infall time decreases again past r_{200} as the halo population is dominated by field galaxies falling in to the cluster for the first time, i.e. infalling halos. These halos can be assigned zero or negative infall times based on estimates for their inevitable infall time onto the cluster (Fig. ??), where a negative median infall time in a particular bin indicates that more than half of the halos have yet to fall in. The tight linear relation between these estimated infall times and r/r_{200} suggests that most field galaxies within r_{200} are falling in to the cluster on nearly direct radial orbits. As a result, despite the scatter in pericentres it is clear in 3D that the infallen halo population can be separated by radial velocity up to an infall time of 2 – 3 Gyr, where these recently infallen halos begin to reach apocenter. Halos with $t_{r200} > 4$ Gyr are almost all part of the virialized population, since few are backsplash galaxies and there is a roughly even split between approaching and receding galaxies.

The trends identified in 3D are less evident in projection. However, the clear distinction between approaching and receding halos remains. Similarly, there are two triangularly-shaped ‘holes’ in the projected phase space, with virtually no halos having infall times between 1 – 2 Gyr within $0.5R_{200}$ and very few backsplash halos with $t_{r200} < 2$ Gyr. If there is a strong environmental impact on infalling galaxies, there should be two distinct populations past R_{200} - currently infalling halos hosting field galaxies and a smaller backsplash population hosting quenched galaxies. Within R_{200} , the distinction is less clear - halos have a variety of infall times, and some are projection effects which have yet to fall in. These projection effects serve to lower the median infall time. As we will demonstrate in Section 4.1, the trends identified in infall time can be mapped onto a stellar population age for halos hosting galaxies undergoing infall-based quenching, which is particularly appropriate for discs. In particular, the sharp drop in median infall time between 0.8-1 R_{200} will cause a similarly large change in optical colours of galaxies for models employing abrupt quenching on infall.

Although there is considerable scatter, subhalo infall times are also correlated with the velocity dispersion and mass of the halo (Fig. 2). The median infall time for dwarf halos ($\sigma < 50 \text{ km s}^{-1}$) is 2-3 Gyr, while almost all massive subhalos ($\sigma > 150 \text{ km s}^{-1}$) fell in at least 2 Gyr ago with a median of 6 Gyr. This can be interpreted as a consequence of the spatial correlation/clustering of overdensities in the early universe, such that the largest overdensity collapsed into the cluster itself while nearby overdensities formed massive subhalos which fell in at early times. The consequences of this correlation on galaxy formation models are that even a purely environmentally-quenched model would predict a non-zero slope in the colour-magnitude relation, since more massive (and hence brighter) galaxies would have fallen in earlier and hence be redder on average.

In addition to the mass trend, there is a weak but non-zero trend in the median velocity dispersions of halos as a function of cluster-centric distance (Fig. 3), even in projection. This can be viewed as a combination of the infall time versus position (Fig. 1) and infall time versus mass relation (Fig. 2), which essentially causes mass segregation of subhalos. One would then expect a model without any explicit environmental dependence to maintain some age trend, as

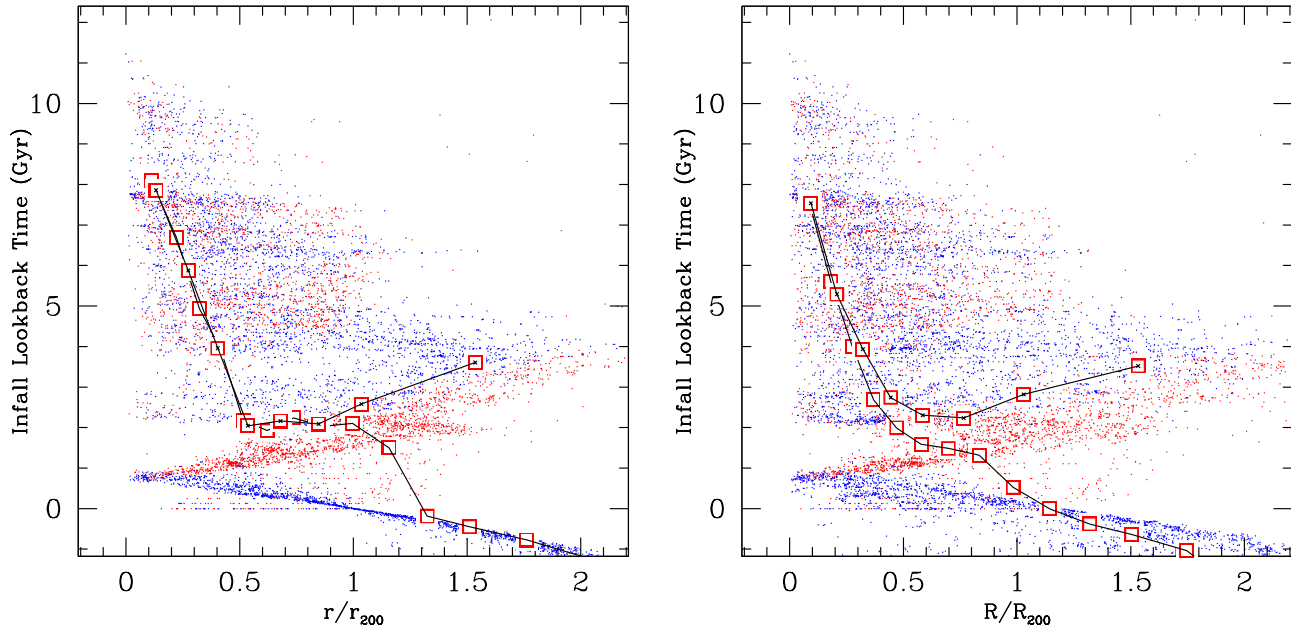


Figure 1. Lookback time at infall t_{r200} for subhalos as a function of radius, in three dimensions (left panel) and in projection (right panel). Halos are colour coded on whether they are approaching (blue) or receding from (red) the cluster. Halos that have not fallen in yet are given a naive estimate of their eventual infall time assuming no changes in their current radial velocity and the size of the cluster. Empty squares show the median infall times for all halos; squares with an x inside show median infall times for only those halos that have fallen in ($t_{r200} > 0$).

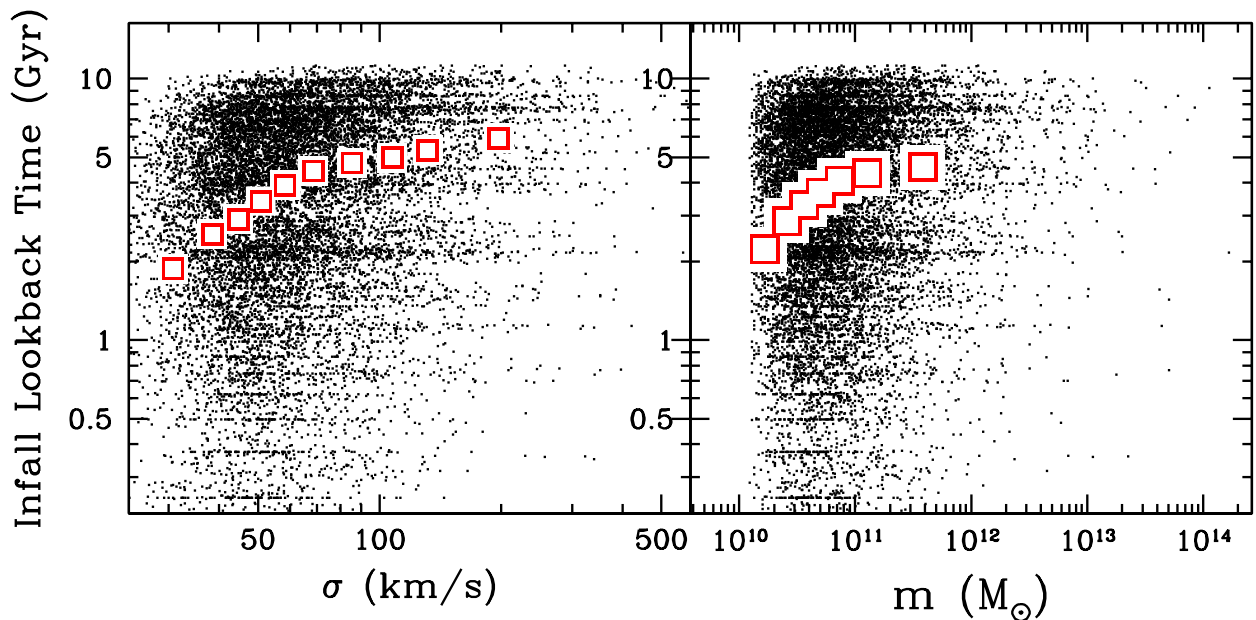


Figure 2. The median lookback times at infall of subhalos as a function of pre-infall velocity dispersion (left panel) and pre-infall mass (right panel). The squares show the median infall times.

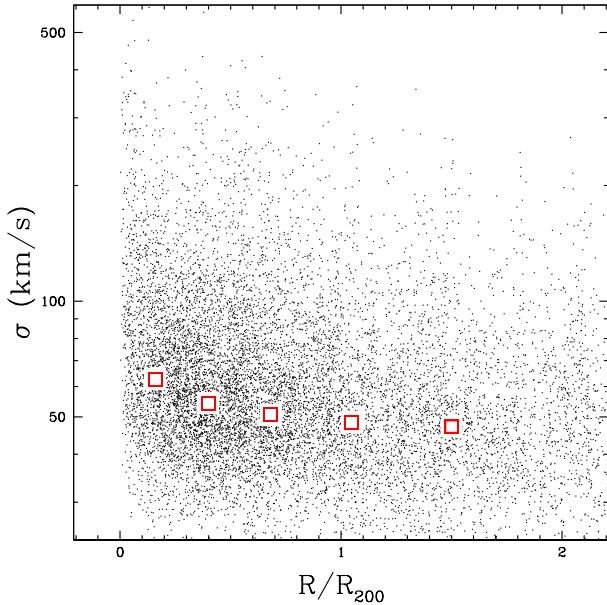


Figure 3. The projected spatial distribution of subhalos as a function of velocity dispersion. The squares show the median velocity dispersion at various radii. Massive subhalos tend to be found near the cluster centre, where the median velocity dispersion is $\sim 20 \text{ km s}^{-1}$ greater than in the field.

long as the quenching is tied to halo mass or velocity dispersion.

3 DATA

Data for giant galaxies in clusters are based on the NOAO Fundamental Plane Survey (Smith et al. 2004, hereafter NFPS) of ~ 3000 galaxies in 94 nearby rich clusters. Colours for 750 giant ($M_R < -20.25$) galaxies in 8 rich clusters are taken from Hudson et al. (2010). This sample has no colour selection and includes red and blue galaxies. It provides (total) galaxy colours in $B-R$ as well as colours in the same filters for the bulge and disc components separately. Spectroscopic data, in the form of central absorption line indices, are from Nelan et al. (2005). The NFPS spectra are too noisy to obtain ages and metallicities for individual galaxies, but the trends as a function of internal velocity dispersion σ and projected distance from the cluster centres are well determined (Smith et al. 2006).

4 STAR FORMATION MODELS

We will now use the halo orbits of Section 2.2 as input to simple star formation models in which environmental, or more specifically cluster-centric “triggers” (such as infall past r_{200} , or pericentre passage) quench star formation. This quenching can either be slow (e.g. causing an exponential decay in the star formation rate), or abrupt. To generate galaxy catalogues from the dark-matter only simulation, each subhalo is assumed to host a single galaxy, and the final simulated galaxy catalog contains only those galaxies with

model stellar populations matching the observational limits of the data, i.e. $M_R < -20.25$. This typically results in a median velocity dispersion limit of $\gtrsim 100 \text{ km/s}$, or $M_{\text{stellar}} \gtrsim M_{\odot} \times 10^{10}$. The subhalos that host these galaxies have masses $M_{\text{halo}} \gtrsim 10^{11} M_{\odot}$.

4.1 Single-component toy models

We first explore two simple toy models designed to test the influence of cluster-centric environment. These are “single component” models in which the entire stellar population of the galaxy is described by a single star formation history (SFH). In Section 4.2 below we will explore more realistic bulge/disc models.

4.1.1 The AHS Models

We will use the Allanson et al. (2009, hereafter AHS) SFH models as baselines for our single-component models. The AHS models parametrized the SFH in terms of simple functional forms (e.g. single burst, exponential, constant SF followed by “abrupt quenching”, etc.) and then adjusted the parameters of the model in order to reproduce both the median and the scatter in the global colours and central spectroscopic line indices of NFPS red-sequence galaxies. Several studies (Smith et al. 2009b; Graves et al. 2009) have shown that stellar populations are more tightly linked to the velocity dispersion than to the stellar mass, so *a priori*, one expects a correlation between mean stellar age and the stellar velocity dispersion. In the AHS models, the central stellar velocity dispersion determines (1) an age-related parameter, such as a Single Stellar Population (hereafter SSP) age or a quenching time, (2) the metallicity and (3) the α -enhancement. Random scatter is added to each of these parameters to generate a galaxy population with a distribution of ages, metallicities and α -enhancements. For each simulated galaxy, the stellar population parameters are used to generate simulated colours and absorption linestrength indices calculated by convolving simple stellar population (SSP) model SEDs (Maraston 1998, 2005) and Lick-index absorption linestrengths (Thomas et al. 2003) with a given SFH in order to reproduce the line indices of red-sequence cluster galaxies from Nelan et al. (2005) and Smith et al. (2007). Having done so, AHS find reasonable agreement with galaxy colours as well. Furthermore, the AHS models include synthetic total magnitudes, allowing us to select samples in the same way as the real NFPS data. Thus by construction the AHS models match the observed red-sequence stellar population observables.

4.1.2 Internal Quenching versus Quenching on Cluster Infall

The first (“null hypothesis”) model is one in which the cluster environment has no direct effect: we assume that the star formation history depends *only* on internal properties of the subhalo (specifically the velocity dispersion of the subhalo), and not on infall into the cluster. The subhalo’s velocity dispersion before cluster-infall is used a proxy for the stellar velocity dispersion. Star formation rates are modelled either

as declining until a specified time t_{AQ} or as a single instantaneous burst (SSP). The α -enhancement and metallicities are assigned through a lookup table of similar galaxies in the AHS mock catalogues. This yields a red-sequence in which stellar population age, and hence galaxy colour, depends only the *internal* properties and not explicitly on position in the cluster. Nevertheless, colours of galaxies in this model have a weak and indirect dependence on cluster-centric radius due to the correlation between subhalo velocity dispersion and cluster-centric radius noted in Section 2.

In the second simple model, the galaxy’s internal velocity dispersion has no effect on its age and metallicity. Instead, the quenching time is set to the lookback time at which it fell into the halo, i.e. the time at which it first crossed r_{200} . Metallicities and α -enhancements are set to solar with small (< 0.05 dex) scatter. To simulate this in the mock catalogues, we draw a galaxy from the AHS mock catalogues that has a similar t_{AQ} as its infall time (independent of the galaxy velocity dispersion).

Quenching can be accomplished in a variety of different ways. In these simple models, quenching is instantaneous and complete. Quenching can alternatively be modelled as an exponential decline in star formation rate with some post-infall e -folding time τ_{post} . Similarly, one might imagine that environmental effects are weak at r_{200} and grow stronger at higher intra-cluster medium densities or simply higher densities for tidal stripping. To approximate this effect, we also consider models where quenching begins at pericentre, where densities should be highest. To briefly distinguish between these models, Table 2 summarizes acronyms and general properties of these parameterizations, all of which will be elaborated upon. For the moment, however, it is instructive to consider only the simplest mass-dependent MSSP and infall-dependent IAQ models to determine if further additions to the models are necessary.

Fig. 4 shows the comparison of the cluster-centric colour gradients for these simple single component models compared to the NFPS global, disc and bulge colours. The internally-quenched model has a very weak colour gradient, in contrast with the steeper dependence on cluster-centric radius in the total colours in the NFPS data. This weak gradient is, however, a much better match to the bulge colours, with the caveat that our models slightly underestimate metallicities and produce an offset of about 0.05. The small variation in colours that is seen is the expected second-order effect produced by the correlation of position with velocity dispersion (Fig. 3), in turn caused by mass segregation (see Section 2.2). If more massive galaxies are also redder, as they are in the NFPS data, a (weak) negative gradient with cluster-centric position results.

A purely infall-based model will typically produce a wider range of galaxy colours and a steeper dependence of colour on cluster-centric radius. Galaxies that have recently (or never) fallen in have the bluest colours, dominating the outskirts of the cluster. In the core of the cluster, the time since infall spans a range from several hundred Myr for the most recently infallen halos still on their first orbit around the cluster core, to many Gyr for older infallen halos now bound to the cluster core, if not virialized. Hence the overall colour gradient is a function of the relationship between infall time and position (Fig. 1) modulated by the dependence of colour on infall time. The former relation is almost

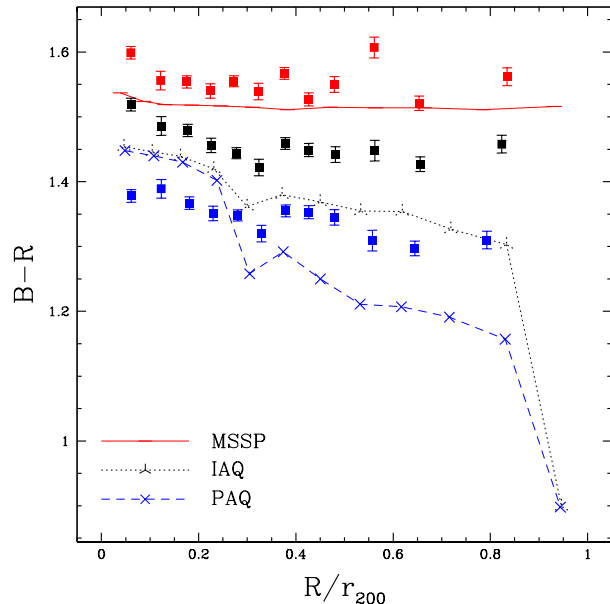


Figure 4. Single component model galaxy colours as a function of projected cluster-centric radius. These simple models include an old single stellar population, abrupt quenching on infall and abrupt quenching at pericenter. Black squares are NFPS total colours; blue are disc and red bulge colours. Error bars for the NFPS data show the uncertainty of the median colour of galaxies in each bin.

entirely determined by cosmology, while the latter is dependent entirely on our choice of star formation model. These abruptly quenched models have steeper colour gradients as a function of cluster-centric radius than both total colours and disc colours, regardless of where quenching occurs (Fig. 4).

We conclude that these toy models bracket the range of possible formation histories for galaxies but are too simplistic to reproduce observed galaxy colours. We now turn to more realistic bulge/disc models that are more complex variants of these simple toy models.

4.2 Bulge plus disc models

4.2.1 Environmental Dependence of Bulges and discs

The $B - R$ colours of bulge and disc components of giant galaxies in clusters were studied by Hudson et al. (2010). They found that bulge colours were redder than discs (as expected) but that bulge colours were independent of cluster-centric radius. In contrast, the colours of disc galaxies depend significantly on cluster-centric radius and drive the weaker trend of global colours as reproduced above (Fig. 4). The lack of radial dependence of the bulge colours is therefore similar to the predictions of the “internally-quenched” toy model above, whereas the radial dependence of the disc colours is similar to the infall-quenched toy model. This suggests that we build a composite bulge/disc model in which only the discs are affected by environment.

In the NFPS data, the bulge-to-disc ratio varies along the red sequence, with higher-mass systems being more bulge-dominated. Indeed AHS showed that the bulge-to-total light ratio (B/T) was tightly correlated with central

Model Name	Acronym	Quenching Method	Quenching Model	Quenching Position	Pre-Infall τ Gyr	Post-Infall τ Gyr
Simple Stellar Population	MSSP	Mass	SSP	N/A	N/A	N/A
Quenched at Infall	IAQ	Infall	AQ	$r/r_{200} = 0.125 - 1$	$\infty - 1$	0
Quenched at Pericentre	PAQ	Pericentre	AQ	$r/r_{200} < 0.125 - 1$	$\infty - 1$	0
Strangled at Infall	IS	Infall	STR	$r/r_{200} = 0.125 - 1$	$\infty - 1$	0.5-7
Strangled at Pericentre	PS	Pericentre	STR	$r/r_{200} < 0.125 - 1$	$\infty - 1$	0.5-7

Table 2. Basic Star Formation Model Parameters.

velocity dispersion (see their Figure A1). We use their empirical relation to determine B/T at a given velocity dispersion σ .

4.2.2 Bulge Model

Having fixed the bulge fraction, bulge ages are then generated as for the “internally-quenched” toy model described above. The bulge metallicity is determined by choosing the total metallicity as a function of its velocity dispersion, by drawing galaxies at random from the AHS models. In practice this means that the bulge has super-solar metallicity and is increasingly metal-rich at larger velocity dispersions. By contrast, discs are solar metallicity with small (< 0.05 dex) scatter and no α -enhancement. Since the total metallicity is a mass-weighted average of the disc and bulge metallicities, we adjust the bulge metallicity to reproduce the desired total metallicity, with a corresponding increase in the bulge α -enhancement.

4.2.3 Disc Quenching Model

The above prescriptions fix the stellar populations of the bulge and also the metallicity and α -enhancement of the disc. This leaves only the SFH of the disc to be modelled. We first consider disc colours in the field, where there is assumed to be no quenching. For field discs, we adopt an exponentially-decaying SFH and constrain the e -folding timescale so that the colours match the median colour of discs in the field: $B - R = 1.25 \pm 0.05$ (Hudson et al. 2010). This is in reasonable agreement with the colours found by MacArthur et al. (2004) for discs in field spiral galaxies in the same magnitude range as the NFPS sample. We find that the observed colours can be fit with a (pre-quenching) exponential timescale $\tau_{\text{pre}} = 4 - 5$ Gyr which yields $B - R$ in the range $1.28 - 1.20$.

In our bulge/disc models, disc quenching will be caused by interaction with the cluster environment. There are two parameters that control the quenching. The first parameter controls how *rapid* the quenching is. In the simplest scenario, star formation is instantly and completely suppressed, as might be expected if the quenching is due to ram-pressure stripping of cold gas. We refer to this as “abrupt” quenching (AQ). Alternatively, star formation may be quenched more gradually, as in the “strangulation” scenario. We model this as a second exponential decay in the star formation rate. The exponential decay time *after* quenching, τ_{post} , is uncertain

and so below we experiment with different values. Note that in this context AQ corresponds to $\tau_{\text{post}} = 0$.

Two additional parameters control how quenching proceeds. One parameter determines *where* in the cluster quenching first occurs: at r_{200} (I) or at pericentre (P). An additional parameter “R” determines how far the influence of the cluster stretches as a factor of r_{200} . By default and in most models this parameter has a value of one; if not otherwise specified this default value applies. In some models, however, R can be smaller than one. In the case of $R = 0.5$, only halos which cross $0.5r_{200}$ are considered as infallen and hence quenched, so halos with pericentres at $0.6r_{200}$ would not be quenched.

4.2.4 Abrupt Quenching or Strangulation?

We first examine the simplest case of abrupt quenching (AQ), setting the pre-infall e -folding time to $\tau_{\text{pre}} = 4$ Gyr. For the moment, we compare only pericentre-quenched models; we will examine the differences between pericentre and infall quenching shortly. We find that the abrupt quenching at r_{200} produces a very sharp transition from blue (star-forming) to red (quenched) galaxies just within the quenching radius, as shown in Fig. 5. We have experimented with different quenching radii (e.g. at a fixed fraction of r_{200} , or at pericentre) and find that changing the quenching radius does not alter sharpness of the transition from blue median colours to red, it merely shifts radius at which the sharp transition occurs. Such a sharp transition is not observed in the NFPS disc colour data. Thus, it is not possible to match the distribution of colours in the colour versus projected position plot with any model that quenches star formation instantly, regardless of where the quenching takes place. This suggests that the disc star formation is quenched more gradually, as might be expected in a “strangulation” model. Furthermore, the location of the transition in median colours is not necessarily the same as that of the quenching radius. Since most galaxies reach pericentre at $0.4r_{200}$, backplash galaxies can dominate out past $0.5r_{200}$. Only by shrinking the quenching radius below $0.4r_{200}$ can a significant change in the transition point be achieved.

Fig. 6 compares strangulation models in which the disc quenching occurs at pericentre (assuming pericentre is within r_{200}) and with different values of pre- and post-quenching τ . These models produce roughly linear median disc colour-position relations, bracketing the slope of the observations. Note that the choice of τ_{pre} fixes the median disc colour of the *outermost* bin of field-dominated galaxies while

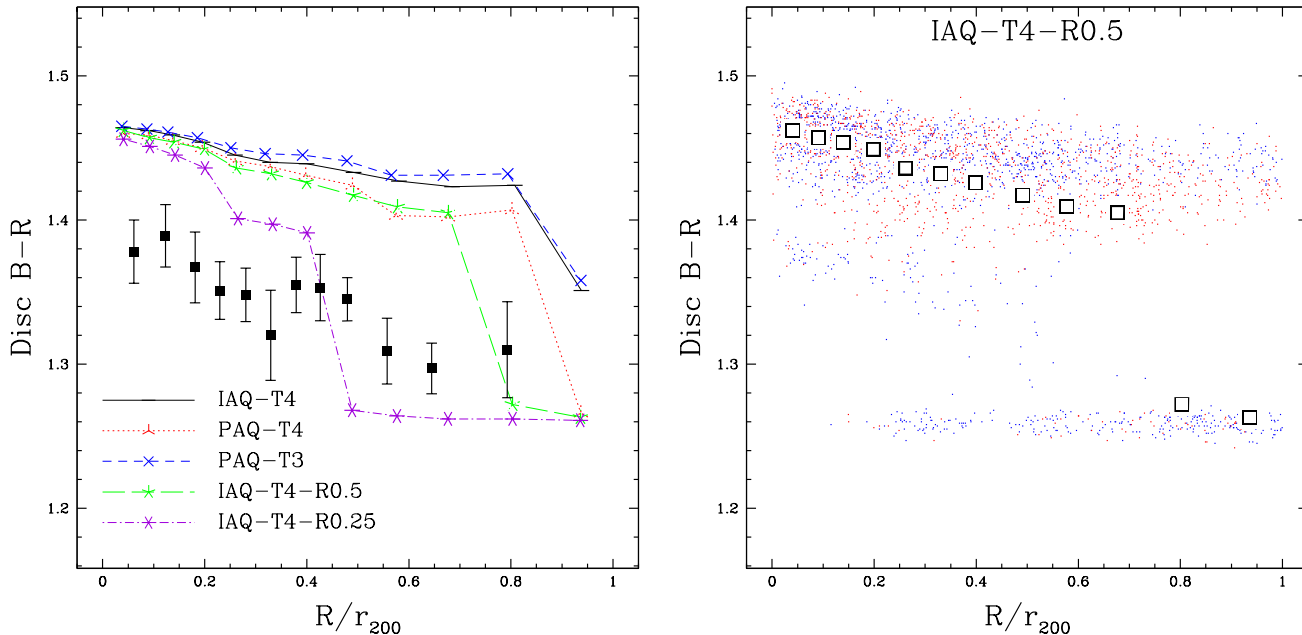


Figure 5. The left panel shows median *disc* colour as a function of projected cluster-centric radius for the NFPS observations (black squares as in Fig. 4) and “abrupt” ($\tau_{\text{post}} = 0$) quenching models. The right hand panel shows the distribution of disc colours for quenching at $0.5r_{200}$ illustrating the sharp transition from star forming to quenched galaxies. Blue points represent galaxies approaching the cluster center in 3D while red are receding.

only slightly altering the colour of the innermost, quenched galaxy-dominated bin. In other words, central cluster galaxies retain little memory of their initial conditions in these models; instead, their colours are most sensitive to τ_{post} , the speed of the quenching after infall. Models with $\tau_{\text{post}} < 2$ Gyr produce discs that are too red compared to galaxies in the innermost radial bin. The model with the closest match to the observations has $\tau_{\text{post}} = 2.5$ Gyr, only slightly faster than the pre-quenching $\tau_{\text{pre}} = 4$ Gyr. This suggests that *on average* quenching need not be especially strong to reproduce the observed trends, and it certainly does not appear to be “abrupt”. However, some quenching must be applied, as models with identical τ_{pre} and τ_{post} produce no colour gradient whatsoever.

The strangulation models also do a reasonable job reproducing the entire disc colour distribution and do not show the strong bimodality in galaxy colours exhibited by the abrupt quenching models in Fig. 5. Such a bimodality could be accommodated in a model with larger dispersions in galaxy metallicities and/or τ_{pre} , which might also be necessary to produce some of the very blue observed discs. Similarly, the observational uncertainties on individual galaxy disc colours of ~ 0.1 mag (Hudson et al. 2010) precludes the rejection of any model with strong colour bimodality. However, strangulation models are particularly attractive because the bimodality visible in colours as a function of 3D cluster-centric distance is virtually completely erased in 2D distances by projection effects, and so no additional adjustments are required to produce a relatively smooth radial dependence of galaxy colours on projected distance. Note, however, that independent evidence exists for strong bimodality in specific star formation rates of galaxies, which we will address in Section 4.2.6.

4.2.5 Quenching Location in the Cluster

In the models discussed above and presented in Fig. 6, the strangulation is assumed to occur at pericentre, where the cluster’s tidal field (and tidal stripping) is strongest. It is possible that a different mechanism is at play. For example, ram pressure stripping is sensitive to the density of the intracluster medium, which depends primarily on radius. We therefore consider whether strangulation models could be compatible with infall-based quenching at radii smaller than r_{200} . Figure 7 shows the median colours for the best fit with $\tau_{(\text{pre},\text{post})} = (4, 2.5)$ model. Strangulation at $0.5r_{200}$ produces virtually indistinguishable results from strangulation at pericentre. Both models predict mostly blue discs near the outskirts and red discs near the cluster center. The model with strangulation at $0.5r_{200}$ produces slightly bluer colours between $0.3 - 0.4r_{200}$, where halos are more likely to have fallen in to $0.5r_{200}$ than to have reached pericentre, and so are slightly younger with an infall quenched model.

Infall-quenched models with very small quenching radii ($r_{\text{quench}} < 0.5r_{200}$) tend to produce a steep transition from the red cluster core to blue, unquenched galaxies. The median colour becomes flat at about 1.5 times the quenching radius. We note that the observations are not inconsistent with such a flat slope from $0.6 r_{200}$ out to the field, in part due to poor statistics on the field population and large error bars on their median disc colours. Thus, we can only safely exclude models with quenching radii much smaller than $0.5 r_{200}$.

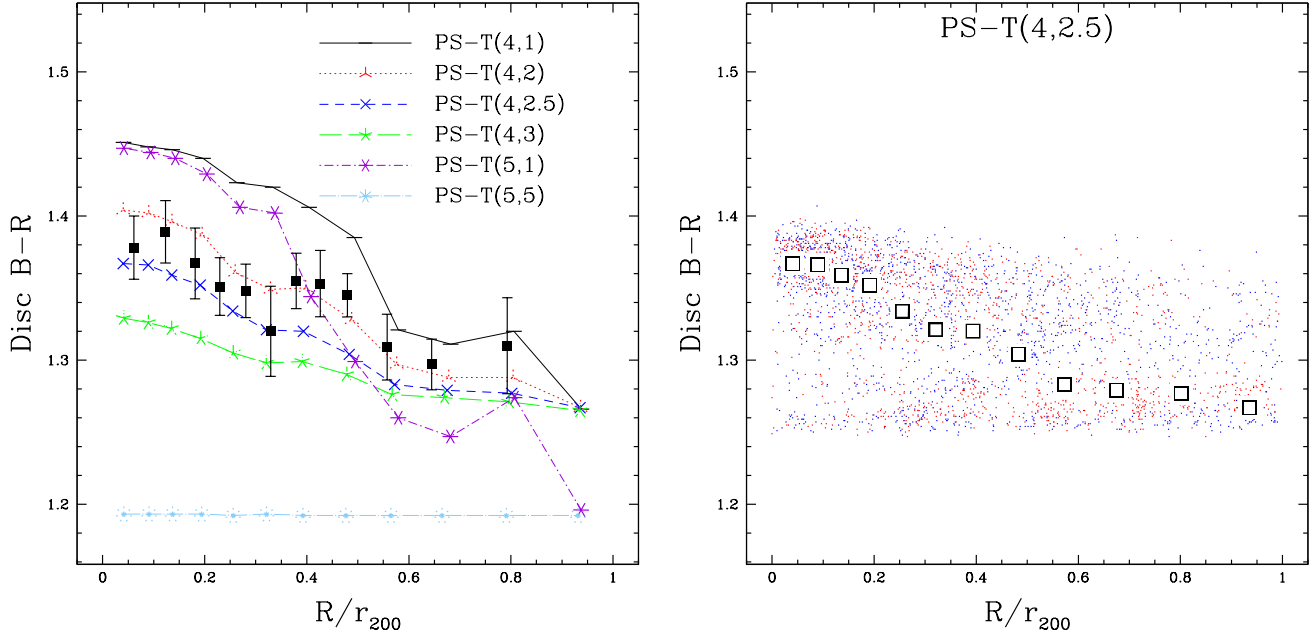


Figure 6. The left panel is as in Fig. 5 but the models are now “strangulation” models in which the disc is exponentially quenched after reaching pericentre. The right-hand panel shows the distribution of disc colours for the PS-T(4,2.5) model. The post-quenching “tail” of star formation (strangulation) results in a steady decrease in median colours of galaxies.

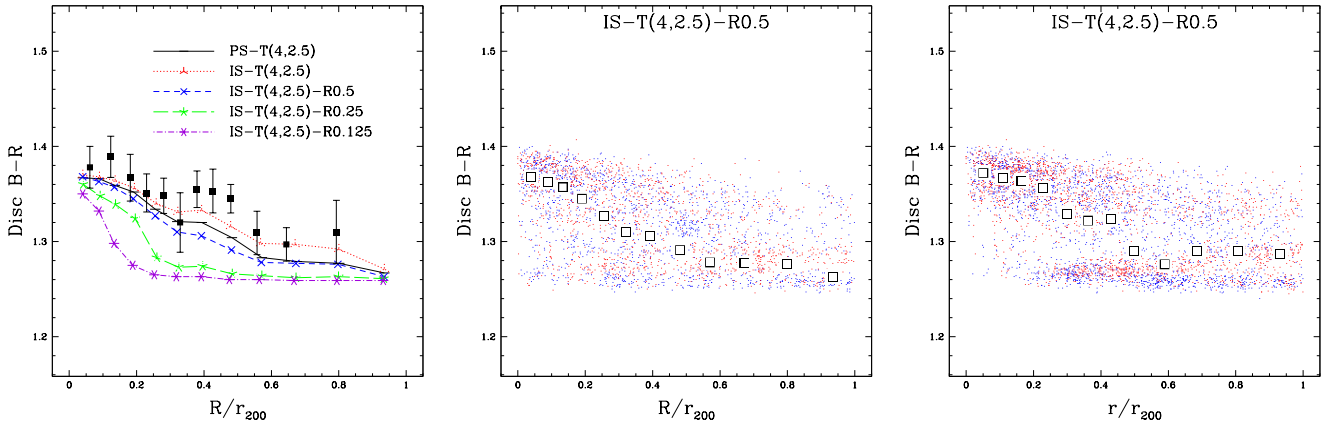


Figure 7. Left panel as in Fig. 5 but now for “strangulation” models invoked at different quenching radii. Only galaxies falling within some fraction of the virial radius are quenched; the smaller the fraction, the closer to the cluster centre the transition from blue- to red-dominated galaxies occurs. The middle and right-hand panels show the distribution of galaxy colours for the IS-T(4,2.5)-R0.5 model as a function of radius (projected and 3D, respectively), illustrating how projection effects wash out the sharp transition in galaxy colours visible in three dimensions.

4.2.6 Delayed Quenching and Bimodality

In a similar study to this one, Wetzel et al. (2012b) found good agreement with SDSS observations of specific star formation rates (SSFRs) using models with “delayed-then-rapid” quenching. The rapid quenching preserves the bimodality in the SSFRs observed by Wetzel et al. (2012a), whereas the delay is necessary to match the overall quenched fraction as a function of environment. Their best fit model has a quenching that begins ~ 3 Gyr after infall, followed by rapid quenching with $\tau_{\text{post}} \sim 0.5 - 1$ Gyr. We implement this by adding a constant delay time to the quenching time. The

effect is similar to pericentre-based quenching, but with a longer delay after infall: pericentre occurs after at most ~ 1 Gyr. After 3 Gyr, galaxies are in the “backsplash” population.

Fig. 8 compares the “delayed-then-rapid” quenching to the strangulation models. The two 3 Gyr delay models (labelled with “-D3”) with $\tau_{\text{post}} = 0.5 - 1$ roughly bracket the range considered by Wetzel et al. (2012b). As expected the additional delay keeps more galaxies on the “blue sequence” compared to a strangulation model with the same τ_{post} . A value of $\tau_{\text{post}} \sim 1$ washed out the abrupt transition of the median colour from blue to red. But a weakness of

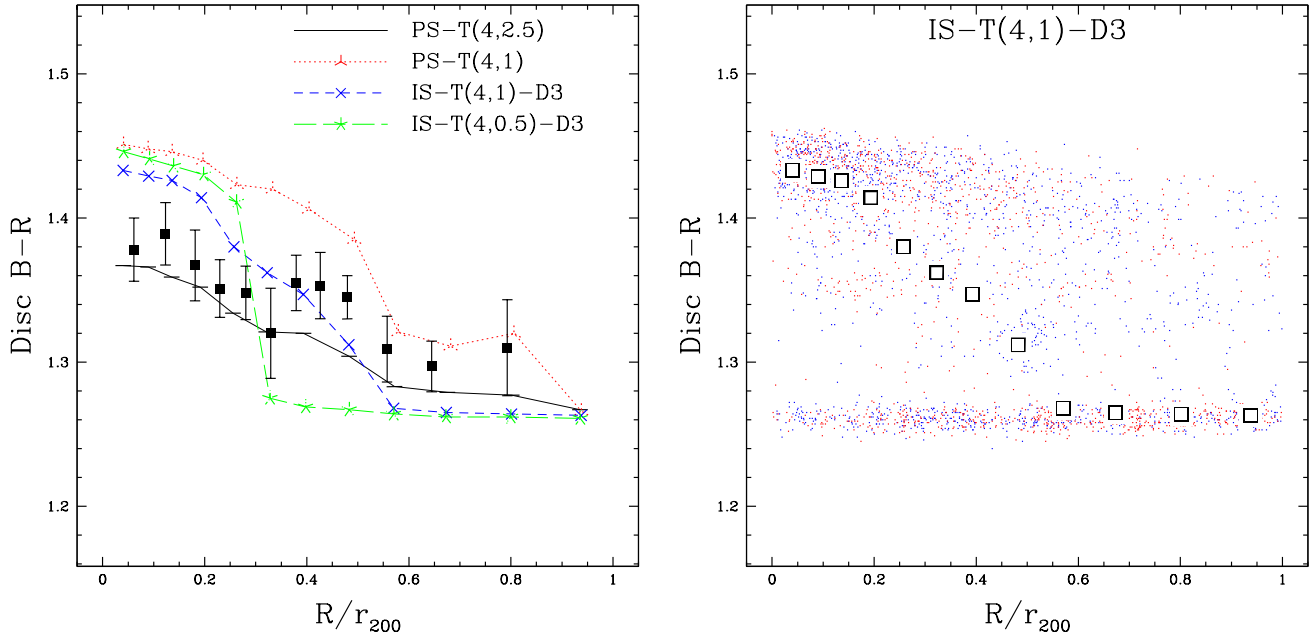


Figure 8. The left panel is as in Fig. 5 but now for "strangulation" models with quenching delayed for a time D after infall/pericentre. The right-hand panel shows the distribution of disc colours for the IS-T(4,1)-D3 model, which displays qualitatively similar behaviour to Fig. 6 but with stronger bimodality and a redder red sequence.

these models is that the mean slope of the $B - R$ vs R/r_{200} is ~ 0.2 magnitudes, whereas the data favour a shallower slope 0.1 ± 0.025 (Hudson et al. 2010). This steep slope is found for *any* model with $\tau_{\text{post}} < 1$, whether delayed or not.

It is interesting to note that the general behaviour of delayed-then-rapid quenching models is to produce a steep gradient in median colours close to the cluster center and a flat slope at larger distances. This is similar to the behaviour found in quenching at small radii (Fig. 7). One might then expect to be able to produce similar results in a model with a small quenching radius, smaller τ_{post} and a delay time in the form of pericentric quenching rather than infall quenching. In fact, the first such model tested produces very similar results to the delayed-then-rapid quenching models, as show in Fig. 8. While these small-radius quenching models do not produce much better fits to disc colours, they do show that one can achieve similar colour bimodality without invoking an arbitrarily long delay in quenching after infall.

In addition to median colours in each bin, we compare the fraction of blue galaxies in different disc models in Fig. 10. Although the choice of division between blue and red is somewhat arbitrary, the blue fractions are similar for all of the models previously shown in Fig. 8, increasing from 15-20 percent near the cluster core to 70-80 percent at R_{200} . The choice of colour cut ($B-R$ of 1.32) can alter the fractions but produces similar results as long as it is between blue sequence and the red galaxies near R_{200} , roughly dividing star-forming from quenched galaxies. The two models with the most similar median colours have virtually identical blue fractions (PS-T(4,1.5)-R0.5 and IS-T(4,0.5)-D3), but curiously two models with quite different trends in median colours also show very similar variations in blue fraction (our fiducial PS-T(4,2.5) model and IS-T(4,1)-D3). In

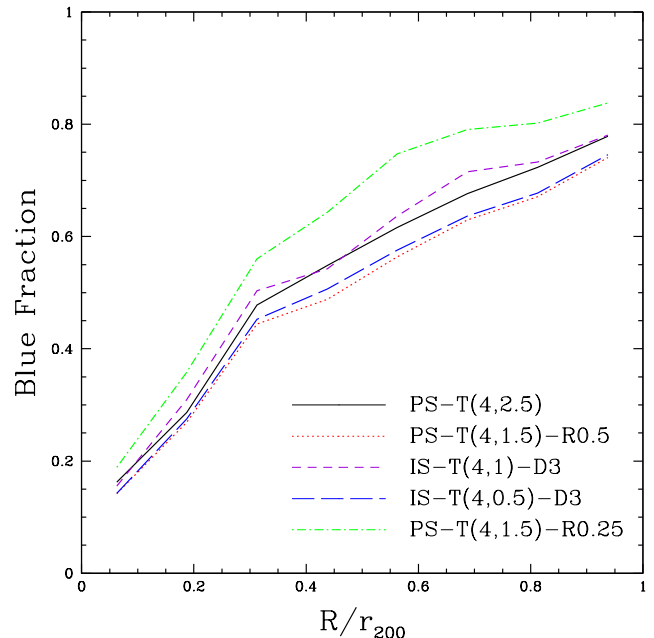


Figure 10. Blue fractions for the disc models in Fig. 9, defined as the fraction of galaxies with colours bluer than the cut of 1.32 separating the blue from the red sequence.

principle one could use the radial trends of blue fractions as an additional diagnostic to validate models. In practice, the uncertainties in observed disc colours are much too large for this exercise, which would also require more careful modelling of the intrinsic scatter in disc colours.

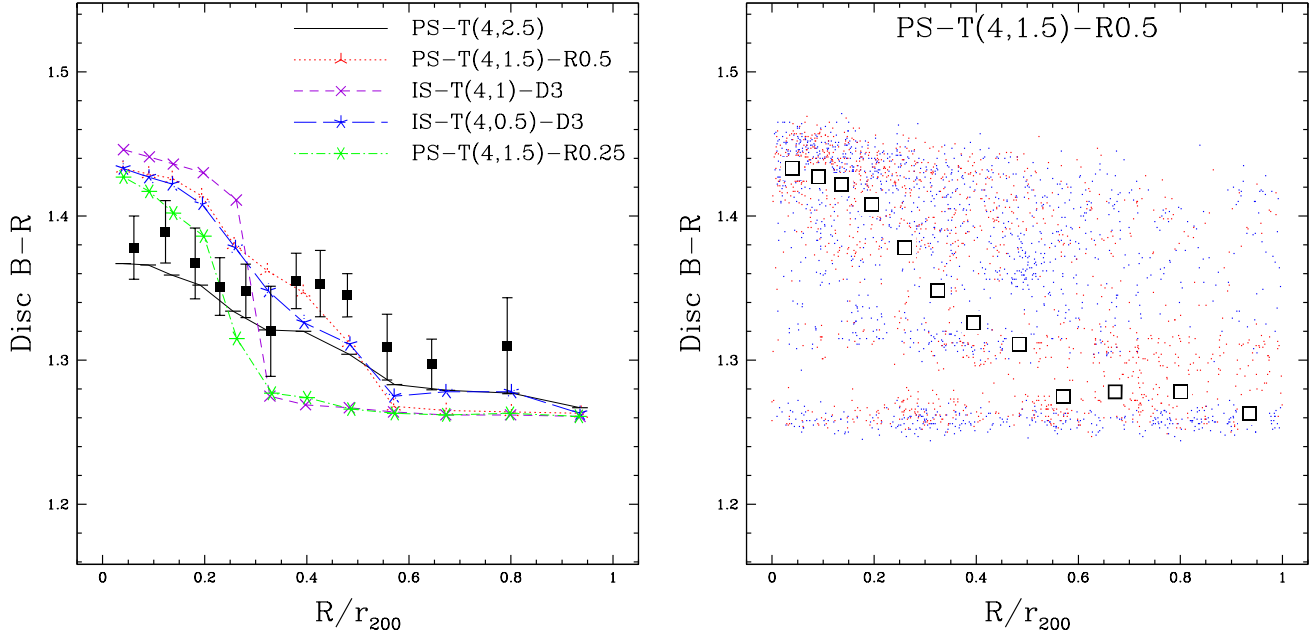


Figure 9. The left panel is as in Fig. 8 but now with additional “strangulation” models with a shorter τ_{post} and a small cluster quenching radius. The right-hand panel shows the distribution of disc colours for the PS-T(4,1.5)-R0.5 model, which displays very similar behaviour to the right panel of Fig. 8.

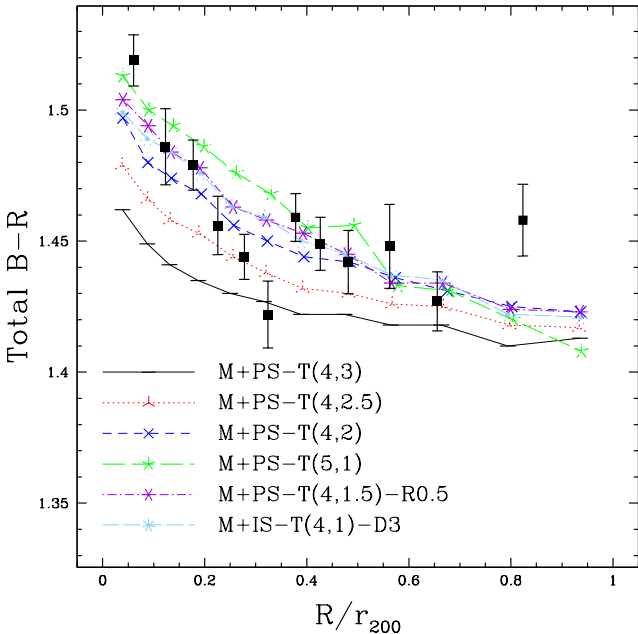


Figure 11. Colours of bulge+disc models compared with NFPS total colours (black points).

4.2.7 Consistency check: total colours

We have shown that a viable model that reproduces both the bulge and disc colours, and their radial dependences, is one in which the bulges are quenched “internally” while discs are quenched by the cluster environment either at pericentre or around $0.5 r_{200}$ and on a timescale of $\tau_{\text{post}} \sim 2 - 3$

Gyr. We can make a further consistency check of this model by comparing total colours of simulated galaxies with NFPS rather than examining discs and bulges separately. Fig. 11 shows the median-colour – projected-distance relation for various two-component models. While none of the bulge-plus-disc models identically reproduce the observed data, they do roughly bracket the range of possibilities, given that the data are not dust-corrected and likely intrinsically somewhat bluer than shown.

4.3 The effect of dust

Galaxy colours are, of course, sensitive to the presence of dust. Driver et al. (2007) find that, on average, bulge+disc galaxies in the field have a some attenuation of B -band light, well-described by a central face-on opacity $\tau_{\text{B}}^f \sim 4$ in the models of Tuffs et al. (2004). It is well known that spiral galaxies in clusters are stripped of HI (Solanes et al. 2001). If dust is also stripped, then this would introduce a difference in colour solely due to the absence of dust in the clusters compared to its presence in field galaxies. Using the models of Tuffs et al. (2004), we estimate that if all the dust was completely stripped, the effect on disc colour would be to make the discs bluer by 0.10 to 0.22 magnitudes in $B - R$ (with a median of 0.14 for a typical disc with an inclination $i = 60^\circ$). Moreover, if the discs on the outskirts were not stripped (and hence contained dust and were redder) and the ones in the centre were stripped (and hence bluer), then the effect would be to make observed gradients shallower. Thus it is possible that the intrinsic (dust-free) cluster-centric gradient in disc colour is considerably steeper than the observed one.

There are, however, two arguments against such an ex-

treme scenario. First, according to the models of Tuffs et al. (2004), the bulge light (and bulge colour) are also strongly affected by dust. If the dust is stripped then the bulge will also appear bluer, and more so for bulges than for discs. In their models, for a typical galaxy with a disc inclination of $i = 60^\circ$ the bulge is reddened by 0.35 mag. Thus, if stripping were important, we would expect bulges in the cluster core to be bluer than those at the cluster edges by 0.35 mag. Yet Hudson et al. (2010) show that there is no gradient in bulge colour as a function of cluster-centric radius. While it remains possible in principle that an intrinsic dependence of bulge stellar populations exactly cancels the putative “dust removal” gradient, this seems rather contrived. Rather it suggests that the dust is not stripped in the cluster core.

Second, it is also possible to study dust stripping directly. Cortese et al. (2010) studied dust stripping in Virgo. They found that there was evidence of dust stripping from the outer edges of discs, but the amount of dust stripping was high only in the most extreme “HI-deficient” galaxies ($\text{defHI} > 1$). Galaxies with such high levels of HI-deficiency are very rare in rich clusters, comprising only a small fraction of the spiral galaxy population (Solanes et al. 2001). We conclude that there is no strong evidence for dust stripping due to the cluster environment in the bulk of the infalling spiral population.

4.4 Comparison with stellar absorption line indices

Stellar absorption lines give detailed information on the ages and metallicities of non-star-forming stellar populations. In this section, we will compare the models to the NFPS data for red galaxies. Note that the NFPS spectra are fibre-spectra of the central regions (2 arcsecond diameter fibres). We can predict how much of the light within this central aperture arises from the bulge, and how much is from the disc, by using our bulge/disc model. This calculation has been done by Hudson et al. (2010, see their Appendix A1) who derive an “aperture” B/T as a function of σ , which ranges from 75-100 percent (depending on velocity dispersion) for the NFPS sample. We adopt their empirical scaling here. Given the fraction of light from the bulge and from the disc, we simulate the central spectral line indices observed by NFPS.

The NFPS line index data are for red galaxies only. To exclude the blue cloud in our models, we reject model galaxies bluer than 0.25 magnitudes from the red sequence, which is assumed to have a slope of 0.05/mag. In most cases, the presence of a significant fraction of bulge light ensures that very few galaxies are bluer than this cut.

The median line-index–projected position relation is shown in Fig. 12. $H\beta$ line index trends are consistent with observations for the bulge-plus-disc strangulation models. The $H\beta$ data are rather noisy, but the model that fits best is the one longest with the longest $\tau_{\text{post}} \sim 3$ Gyr. The $H\gamma$ (HgF) data appears to disfavour many of the models. Only the intermediate $\tau_{(\text{pre}, \text{post})} = (4, 3)$ model appears to predict a sufficiently shallow radial gradient to at least marginally agree with the $H\gamma$ data. In particular, the models with short quenching times ($\tau_{\text{post}} \sim 1$ Gyr) predict very steep $H\gamma$ gradients, as the virialized population will have virtually no young stars to produce strong $H\gamma$ absorption.

In summary, the line indices favour slightly longer post infall strangulation times than do the colours. Recall, however, that the fibre data measure only the central 1.9 kpc. We have extrapolated the disc light assuming that it follows an exponential profile right to the centre of the galaxy. The assumption may not be valid, particularly for S0s and early-type spirals. Furthermore, the Balmer line indices are sensitive to *recent* star formation, so what is relevant here is actually the scale lengths of the star-forming part of the exponential disc, which may differ from the R -band scale length used in the bulge-disc model. Koopmann et al. (2006) found that $H\alpha$ was more extended than R -band light, at least in late-type galaxies in the field. Similarly, UV and blue colour gradients also suggest that, on average, recent star-formation is occurring preferentially in the outer disc (Muñoz-Mateos et al. 2007), particularly in HI-rich galaxies (Wang et al. 2011). The situation for earlier-type galaxies and cluster galaxies is the less clear, but does suggest that the possibility that the central regions have less star-forming disc light than the simple exponential extrapolation used here.

5 DISCUSSION

We have shown that models with relatively rapid quenching fail to match the observations. By relatively rapid quenching, we mean either “abrupt” quenching, which corresponds to $\tau_{\text{post}} = 0$, or “strangulation” models with $\tau_{\text{post}} \leq 1$ Gyr. Such models fail in two ways. First, for galaxies in the centres of clusters, these models produce discs which are redder than observed, and a cluster-centric radial gradient in disc colours which is too steep (Fig. 5). Second, they overpredict the Balmer lines (Fig. 12). These basic trends are present whether the quenching occurs at infall or a fraction of r_{200} or is delayed.

Models in which star formation is quenched more slowly (2-3 Gyr) do a better job at reproducing both the disc colour cluster-centric radial gradients and the absorption line trends. The colour data prefer timescales at the shorter end of the range (~ 2 Gyr) whereas the absorption linestrengths prefer $\gtrsim 3$ Gyr timescales.

It is more difficult to determine where in the cluster the quenching is triggered. Models in which strangulation begins at the virial radius or at pericentre are equally good fits to the disc colour gradients, but the latter has better physical motivation. However, the difference between otherwise identical models employing quenching on infall vs pericentre is typically quite small, and the models can easily accommodate quenching at some intermediate point in the orbit as well.

We can also compare the quenching times in our best-fit models to those quoted in other recent works employing environmental quenching. Wang et al. (2007) modelled quenching of satellite galaxies, favouring an e-folding time (i.e. τ_{post} of 2.5 Gyr, similar to our own best fits. De Lucia et al. (2011) presented models suggesting that satellites on average spend 5-7 Gyr within a halo of mass $m > 10^{13} M_\odot$ before being quenched. Although such models are not directly comparable to our own, as we only allow the cluster itself to quench subhalos, a 5-7 Gyr quenching time is not entirely inconsistent with some models depending on when one considers a galaxy to be quenched. For example,

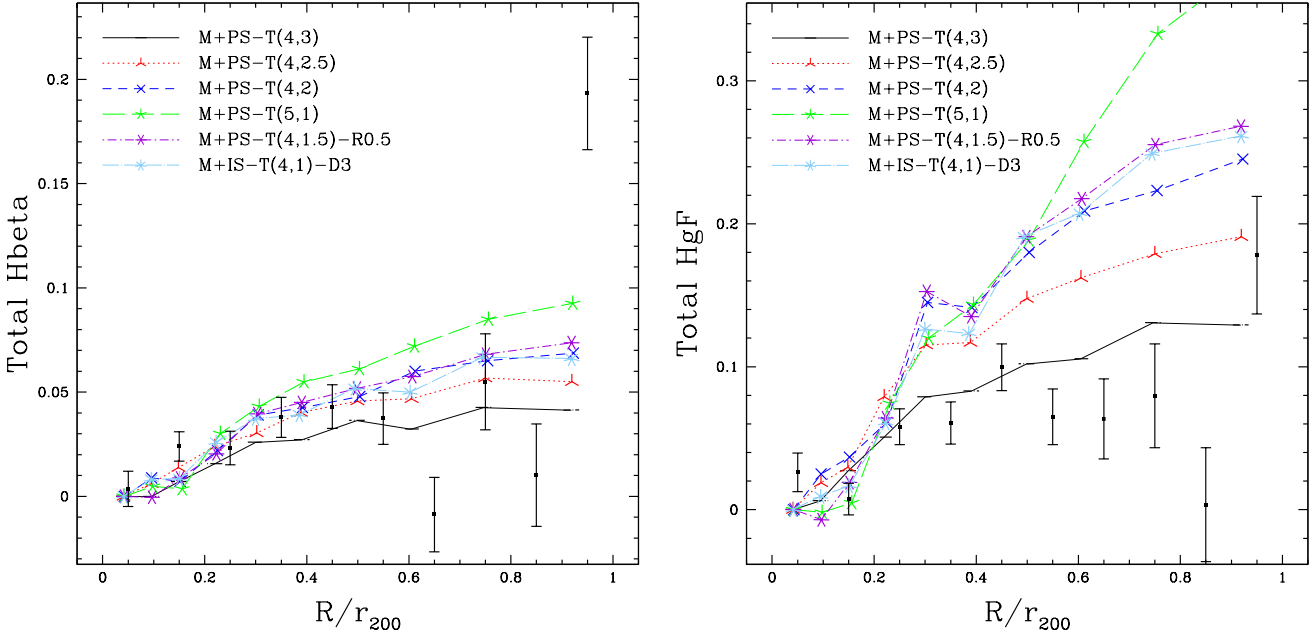


Figure 12. Differential stellar absorption line indices as a function of projected position. The left panel shows $H\beta$ and the right panel shows $H\gamma$. The vertical axis is the *residual* from the mean line index- σ relation, normalized to 0 at $R = 0$. NFPS data for giant red galaxies (Smith et al. 2006) are shown by the black squares with error bars. The curves show bulge-plus-disc models for red galaxies with disc strangulation at pericentre, but differing pre- and post-infall timescales. For example, the black solid curve labelled M+-PS-T(4,3) has a $\tau_{\text{pre}} = 4$ Gyr and $\tau_{\text{post}} = 3$ Gyr and is a good fit to the $H\beta$ cluster-centric radial gradient, and only slightly overpredicts the $H\gamma$ gradient. The other curves have shorter post-infall quenching times and are poorer fits.

in the $\tau_{\text{post}} = 3$ Gyr model, it would take nearly 7 Gyr for star formation to drop to 10 percent of its pre-quenching value after reaching pericentre.

Several recent studies (Weinmann et al. 2010; Wetzel et al. 2012b) have attempted to reproduce the observed bimodality in specific star formation rates (SSFRs) in SDSS galaxies with (respectively) full semi-analytic models or simple parametric star formation models. The generally-favoured model with $\tau_{\text{post}} \sim 2.5$ Gyr does not produce a strong bimodality in disc or global galaxy colours as a result of the relatively long e -folding time. For this reason, the models of Wetzel et al. (2012b) prefer a short quenching e -folding time, equivalent to our τ_{post} . To avoid producing too many red galaxies, they introduce a ~ 3 Gyr delay before quenching begins. However, as noted above, Fig. 8 shows that the short τ_{post} also produces discs in cluster centres that are too red compared to those at the virial radius. They also predict $H\gamma$ linestrengths for red galaxies near the virial radius that are stronger than observed (Fig. 12).

Although most of our data disfavour models with short τ_{post} and long delay times, we have been able to produce alternative models with similarly (but slightly weaker) colour bimodality (Fig. 9). This is achieved by shrinking the quenching radius, quenching at infall instead of pericentre (producing a short delay), and increasing τ_{post} slightly. These models are perhaps more physically plausible as they do not introduce an arbitrary delay time and there are no particularly strong constraints on whether the quenching radius is closer to 0.5 or $1 \times r_{200}$. Still, these alternative models do not provide much better fits to the colour or line-

index trends, so they do not solve the general problem that the relatively rapid quenching necessary to produce bimodal colours produces discs that are too red.

There are several ways in which these studies could be improved. The overmerging problem can be addressed partially with better numerical resolution. More recent halo finding algorithms use particle velocities in addition to positions and binding energies (Oman et al. 2012), which can improve estimates of infall and pericentre times and pericentre distances. Both of these improvements would likely affect low mass halos containing dwarf galaxies more so than the massive halos in our galaxy sample, which are well resolved. Halo velocities can also be used to disentangle projection effects and backsplash galaxies (Mahajan et al. (2011)), although large observational samples are required to detect significant differences in the data.

Because of our focus on reproducing mean/median trends, we did not include many ingredients into our disc models, such as mass-dependent SFRs, and scatter in the SFHs which one might model as variable τ_{pre} . These ingredients would likely help in reproducing the scatter about the mean relations and better reproducing mass-dependent trends, e.g. for dwarfs vs. giants, for which we do note substantial differences in the infall history. Another missing ingredient in the models is variable or density-dependent quenching strengths. Quenching mechanisms like ram-pressure stripping can depend strongly on intra-cluster gas density, pressure and satellite infall velocity (Gunn & Gott 1972; McCarthy et al. 2008). The inclination of the satellite's disc may also have an impact. These effects could introduce significant scatter in the val-

ues of τ_{post} and explain the more extreme observations of ram-pressure stripping in galaxies.

The models presented here only consider quenching from the cluster itself and neglect pre-processing in smaller groups prior to infall. However, Fig. 2 shows that subhalos massive enough ($\sigma > 200\text{km/s}$) to pre-process their own satellites fell in over 5 Gyr ago. Thus, the galaxies most likely to have been affected by pre-processing are already part of the old, virialized population. Furthermore, our best-fit disc models are tuned to reproduce field galaxies outside of galaxy clusters. These field galaxies include (potentially) pre-processed disc galaxies in groups, and so the disc components in our models reproduce the mean effect of pre-processing by construction.

Despite these caveats, it is rather remarkable that reasonable agreement is found between different models and observational data sets. It is also surprising that models with as few as two free parameters can match galaxy colours and absorption linestrengths from cluster centre to outskirts, though simultaneously matching both observations is difficult. All of our successful models favour relatively gentle environmental quenching with timescales longer than the dynamical time in the cluster and longer than typically quoted for ram-pressure stripping of cold gas discs.

6 SUMMARY

We have constructed a catalog of subhalos in dark matter simulations of four rich cluster of galaxies. By tracking halo orbits, we have demonstrated that the infall history of halos imprints a relationship between two key parameters (infall time and halo velocity dispersion) of halos and their projected distance from the cluster centre. By assigning stellar masses to a single galaxy within each halo, we have also been able to test a variety of models for the star formation histories of cluster galaxies. Novel aspects of this analysis are, first, the comparison with stellar absorption linestrengths and second, the separate consideration of bulge and disc colours, as opposed to global colours.

In our best-fitting models, the bulge component of galaxies is quenched “internally”, i.e. its age is not determined by infall into the cluster and can be fit with an old SSP. The observed colours of the discs of field galaxies require that, prior to infall, the star formation rate declines with a characteristic e -folding time $\tau_{\text{pre}} = 4 - 5$ Gyr. Models with no disc quenching fail to explain the redder colours of discs near the cluster centre. Models with short quenching times produce sharp changes in the median colours of discs and a stronger cluster-centric radial disc colour gradient than is observed. They also overpredict the strength of the Balmer lines. Instead, we favour a model in which the disc continues to experience exponentially declining star formation rates with shorter characteristic $\tau_{\text{post}} = 2 - 3$ Gyr. This is suggestive of a gentler mechanism (e.g. “strangulation”) as opposed to rapid ram-pressure stripping of the cold gas.

7 ACKNOWLEDGMENTS

We thank Gary Mamon for useful discussions. DST was supported in this work by an NSERC USRA and Ontario Graduate Scholarships. MJH and MLB acknowledge support from an NSERC Discovery Grant. RJS was supported for this work by STFC Rolling Grant PP/C501568/1 Extragalactic Astronomy and Cosmology at Durham 20082013.

REFERENCES

- Abadi M. G., Moore B., Bower R. G., 1999, MNRAS, 308, 947
 Allanson S. P., Hudson M. J., Smith R. J., Lucey J. R., 2009, ApJ, 702, 1275
 Auger M. W., Treu T., Bolton A. S., Gavazzi R., Koopmans L. V. E., Marshall P. J., Moustakas L. A., Burles S., 2010, ApJ, 724, 511
 Balogh M. L., Baldry I. K., Nichol R., Miller C., Bower R., Glazebrook K., 2004, ApJL, 615, L101
 Balogh M. L., Morris S. L., 2000, MNRAS, 318, 703
 Balogh M. L., Navarro J. F., Morris S. L., 2000, ApJ, 540, 113
 Baugh C. M., 2006, Reports on Progress in Physics, 69, 3101
 Berrier J. C., Stewart K. R., Bullock J. S., Purcell C. W., Barton E. J., Wechsler R. H., 2009, ApJ, 690, 1292
 Boselli A., Gavazzi G., 2006, PASP, 118, 517
 Bower R. G., Lucey J. R., Ellis R. S., 1992, MNRAS, 254, 601
 Cole S., Lacey C. G., Baugh C. M., Frenk C. S., 2000, MNRAS, 319, 168
 Conroy C., Wechsler R. H., Kravtsov A. V., 2006, ApJ, 647, 201
 Cortese L., Davies J. I., Pohlen M., Baes M., Bendo G. J., Bianchi S., Boselli A., de Looze I., Fritz J., Verstappen J., Bomans D. J., Clemens M., Corbelli E., Dariush A., di Serego Alighieri S., Fadda D., Garcia-Appadoo D. A., Gavazzi G., Giovanardi C., Grossi M., Hughes T. M., Hunt L. K., Jones A. P., Madden S., Pierini D., Sabatini S., Smith M. W. L., Vlahakis C., Xilouris E. M., Zibetti S., 2010, A&A, 518, L49
 Davies R. D., Lewis B. M., 1973, MNRAS, 165, 231
 De Lucia G., Weinmann S., Poggianti B., Aragon-Salamanca A., Zaritsky D., 2011, ArXiv e-prints
 Diaferio A., Kauffmann G., Balogh M. L., White S. D. M., Schade D., Ellingson E., 2001, MNRAS, 323, 999
 Dressler A., 1980, ApJ, 236, 351
 Driver S. P., Popescu C. C., Tuffs R. J., Liske J., Graham A. W., Allen P. D., de Propriis R., 2007, MNRAS, 379, 1022
 Gallagher III J. S., Ostriker J. P., 1972, AJ, 77, 288
 Giovanelli R., Haynes M. P., 1985, ApJ, 292, 404
 Graves G. J., Faber S. M., Schiavon R. P., 2009, ApJ, 693, 486
 Gunn J. E., Gott J. R. I., 1972, ApJ, 176, 1
 Haynes M. P., Giovanelli R., Chincarini G. L., 1984, ARA&A, 22, 445
 Hogg D. W., Blanton M. R., Brinchmann J., Eisenstein D. J., Schlegel D. J., Gunn J. E., McKay T. A., Rix H.-W., Bahcall N. A., Brinkmann J., Meiksin A., 2004, ApJL, 601, L29

- Hubble E., Humason M. L., 1931, *ApJ*, 74, 43
- Hudson M. J., Stevenson J. B., Smith R. J., Wegner G. A., Lucey J. R., Simard L., 2010, *MNRAS*, 409, 405
- Katz N., White S. D. M., 1993, *ApJ*, 412, 455
- Kauffmann G., Colberg J. M., Diaferio A., White S. D. M., 1999, *MNRAS*, 303, 188
- Kauffmann G., White S. D. M., Guiderdoni B., 1993, *MNRAS*, 264, 201
- Klypin A., Gottlöber S., Kravtsov A. V., Khokhlov A. M., 1999, *ApJ*, 516, 530
- Knollmann S. R., Knebe A., 2009, *ApJS*, 182, 608
- Komatsu E., Smith K. M., Dunkley J., Bennett C. L., Gold B., Hinshaw G., Jarosik N., Larson D., Nolte M. R., Page L., Spergel D. N., Halpern M., Hill R. S., Kogut A., Limon M., Meyer S. S., Odegard N., Tucker G. S., Weiland J. L., Wollack E., Wright E. L., 2011, *ApJS*, 192, 18
- Koopmann R. A., Haynes M. P., Catinella B., 2006, *AJ*, 131, 716
- Koopmann R. A., Kenney J. D. P., 2004, *ApJ*, 613, 866
- Larson R. B., Tinsley B. M., Caldwell C. N., 1980, *ApJ*, 237, 692
- MacArthur L. A., Courteau S., Bell E., Holtzman J. A., 2004, *ApJS*, 152, 175
- Mahajan S., Mamon G. A., Raychaudhury S., 2011, *MNRAS*, 416, 2882
- Mamon G. A., 1987, *ApJ*, 321, 622
- Mamon G. A., Biviano A., Murante G., 2010, *A&A*, 520, 30
- Maraston C., 1998, *MNRAS*, 300, 872
- , 2005, *MNRAS*, 362, 799
- McCarthy I. G., Frenk C. S., Font A. S., Lacey C. G., Bower R. G., Mitchell N. L., Balogh M. L., Theuns T., 2008, *MNRAS*, 383, 593
- McGee S. L., Balogh M. L., Bower R. G., Font A. S., McCarthy I. G., 2009, *MNRAS*, 400, 937
- Merritt D., 1984, *ApJ*, 276, 26
- Moore B., Katz N., Lake G., 1996, *ApJ*, 457, 455
- Moore B., Lake G., Katz N., 1998, *ApJ*, 495, 139
- Muñoz-Mateos J. C., Gil de Paz A., Boissier S., Zamorano J., Jarrett T., Gallego J., Madore B. F., 2007, *ApJ*, 658, 1006
- Navarro J. F., White S. D. M., 1994, *MNRAS*, 267, 401
- Nelan J. E., Smith R. J., Hudson M. J., Wegner G. A., Lucey J. R., Moore S. A. W., Quinney S. J., Suntzeff N. B., 2005, *ApJ*, 632, 137
- Oman K. A., Hudson M. J., Behroozi P. S., 2012, *MNRAS*, submitted
- Peng Y., Lilly S. J., Renzini A., Carollo M., 2011, *ArXiv e-prints*
- Peng Y.-j., Lilly S. J., Kovač K., Bolzonella M., Pozzetti L., Renzini A., Zamorani G., Ilbert O., Knobel C., Iovino A., Maier C., Cucciati O., Tasca L., Carollo C. M., Silverman J., Kampeczyk P., de Ravel L., Sanders D., Scoville N., Contini T., Mainieri V., Scodreggio M., Kneib J.-P., Le Fèvre O., Bardelli S., Bongiorno A., Caputi K., Coppa G., de la Torre S., Franzetti P., Garilli B., Lamareille F., Le Borgne J.-F., Le Brun V., Mignoli M., Perez Montero E., Pello R., Ricciardelli E., Tanaka M., Tresse L., Vergani D., Welikala N., Zucca E., Oesch P., Abbas U., Barnes L., Bordoloi R., Bottini D., Cappi A., Cassata P., Cimatti A., Fumana M., Hasinger G., Koekemoer A., Leauthaud A., Maccagni D., Marinoni C., McCracken H., Memeo P., Meneux B., Nair P., Porciani C., Presotto V., Scaramella R., 2010, *ApJ*, 721, 193
- Postman M., Geller M. J., 1984, *ApJ*, 281, 95
- Power C., Navarro J. F., Jenkins A., Frenk C. S., White S. D. M., Springel V., Stadel J., Quinn T., 2003, *MNRAS*, 338, 14
- Sandage A., Visvanathan N., 1978, *ApJ*, 223, 707
- Sivanandam S., Rieke M. J., Rieke G. H., 2010, *ApJ*, 717, 147
- Smith R. J., Hudson M. J., Lucey J. R., Nelan J. E., Wegner G. A., 2006, *MNRAS*, 369, 1419
- Smith R. J., Hudson M. J., Nelan J. E., Moore S. A. W., Quinney S. J., Wegner G. A., Lucey J. R., Davies R. L., Malecki J. J., Schade D., Suntzeff N. B., 2004, *AJ*, 128, 1558
- Smith R. J., Lucey J. R., Hammer D., Hornschemeier A. E., Carter D., Hudson M. J., Marzke R. O., Mouhcine M., Eftekharzadeh S., James P., Khosroshahi H., Kourkchi E., Karick A., 2010, *MNRAS*, 408, 1417
- Smith R. J., Lucey J. R., Hudson M. J., 2007, *MNRAS*, 381, 1035
- , 2009a, *MNRAS*, 400, 1690
- Smith R. J., Lucey J. R., Hudson M. J., Allanson S. P., Bridges T. J., Hornschemeier A. E., Marzke R. O., Miller N. A., 2009b, *MNRAS*, 392, 1265
- Smith R. J., Lucey J. R., Price J., Hudson M. J., Phillipps S., 2012, *MNRAS*, 419, 3167
- Solanes J. M., Manrique A., García-Gómez C., González-Casado G., Giovanelli R., Haynes M. P., 2001, *ApJ*, 548, 97
- Springel V., 2005, *MNRAS*, 364, 1105
- Springel V., White S. D. M., Tormen G., Kauffmann G., 2001, *MNRAS*, 328, 726
- Sun M., Donahue M., Voit G. M., 2007, *ApJ*, 671, 190
- Thomas D., Maraston C., Bender R., 2003, *MNRAS*, 339, 897
- Tormen G., 1997, *MNRAS*, 290, 411
- Tormen G., Diaferio A., Syer D., 1998, *MNRAS*, 299, 728
- Tuffs R. J., Popescu C. C., Völk H. J., Kylafis N. D., Dopita M. A., 2004, *A&A*, 419, 821
- van den Bosch F. C., Aquino D., Yang X., Mo H. J., Pasquali A., McIntosh D. H., Weinmann S. M., Kang X., 2008, *MNRAS*, 387, 79
- Wang J., Kauffmann G., Overzier R., Catinella B., Schiminovich D., Heckman T. M., Moran S. M., Haynes M. P., Giovanelli R., Kong X., 2011, *MNRAS*, 412, 1081
- Wang L., Li C., Kauffmann G., De Lucia G., 2007, *MNRAS*, 377, 1419
- Weinmann S. M., Kauffmann G., van den Bosch F. C., Pasquali A., McIntosh D. H., Mo H., Yang X., Guo Y., 2009, *MNRAS*, 394, 1213
- Weinmann S. M., Kauffmann G., von der Linden A., De Lucia G., 2010, *MNRAS*, 406, 2249
- Wetzel A. R., Tinker J. L., Conroy C., 2012a, *MNRAS*, 424, 232
- Wetzel A. R., Tinker J. L., Conroy C., van den Bosch F. C., 2012b, *ArXiv e-prints*
- Yagi M., Komiyama Y., Yoshida M., Furusawa H., Kashikawa N., Koyama Y., Okamura S., 2007, *ApJ*, 660, 1209
- Yoshida M., Yagi M., Komiyama Y., Furusawa H., Kashikawa N., Koyama Y., Yamanoi H., Hattori T., Oka-

mura S., 2008, ApJ, 688, 918